International Journal of Electromagnetics and Applications 2013, 3(4): 103-119
DOI: 10.5923/j.ijea.20130304.06

Miniaturized Dual-Fractal Antenna Structure for RFID Tags

D. K. Naji[1], R. S. Fyath[2,*]

[1]Department of Electronic and Communications Engineering, College of Engineering, Alnahrain University, Baghdad, Iraq
[2]Department of Computer Engineering, College of Engineering, Alnahrain University, Baghdad, Iraq

Abstract A design approach for the miniaturization of a dual-antenna structure (DAS) for radio-frequency identification (RFID) tag system is presented. The structure contains two radiating elements, one as a receiving antenna and the other as backscattering antenna, printed on the opposite sides of the substrate and perpendicular to each other to keep relatively lower coupling between them. The proposed design procedure contains number of intermediate steps, each of which produces antenna miniaturization as well as the desired impedance matching properties. The DAS is optimized using two softwares coupling to each other: a general computing tool (MATLAB) to implement the particle swarm optimization (PSO) technique and Electromagnetic Simulator (CST Microwave Studio) to extract antenna performance parameters. The aim of the optimization technique is to miniaturize the DAS under two strict conditions, namely maximizing both the feeding power to the IC tag connected to the receiving antenna (conjugate matching) and the backscattered fields difference (making the input impedance of the backscattering antenna pure real). The design approach is applied to both conventional and 3rd-order Sierpinski gasket, with ellipse generation, fractal bow-tie patch antennas and yields 49% and 68% area reduction, respectively, compared with the reference (non-fractal) single-antenna tag counterpart at 5.8 GHz band.

Keywords Bow-tie antenna, Dual-fractal antenna structure, RFID antenna, Particle swarm optimization (PSO)

1. Introduction

Radio frequency identification (RFID) has emerged as one of the most popular methods for asset, person, and object identification through the use of active or passive chipped tag antennas bearing a univocal identification code[1, 2]. In recent years, there has been rapid growth in the development of RFID systems for various applications including industrial fields[3-5]. An RFID system is comprised of tags, readers, and information management system. In developing an RFID solution, the focus is usually placed on designing high performance tags suitable for practical applications[6]. The tag's antenna has to be small in size and light in weight, as it is attached to the objet that would be identified, and should be also inexpensive for mass production[7]. However, the design of RFID tag antennas is a tradeoff between size reduction and performance[8-10].

For most RFID applications, it is strongly desired to maintain a minimal fast print for the tag. Therefore, passive tags attract increasing interest in RFID applications[11, 12]. The fundamental idea of passive RFID system is that the transponder is powered via the air interface by means of magnetic fields or electromagnetic radio waves and hence the system can operate without the use of any external energy storage devices[13, 14]. A typical passive tag consists of an antenna and an application specific integrated circuit (ASIC) chip. The communication between the reader and the passive tag involves two links[15]

i) Forward link: The reader sends out continuous wave (CW) and commands to the tag. The tag chip turns on and responds to the command when it receives sufficient power from the CW.

ii) Backward link: The tag antenna is alternatively connected to two different load impedances according to the data stored in the chip. The CW is modulated in this manner and scattered back to the reader.

To achieve successful communication between the reader and the tag, two conditions must be satisfied simultaneously. First, conjugate impedance matching between the tag antenna and the chip must be exists to ensure maximum power transfer to power the chip. Secondly, the difference between the high and low levels of the backscattered wave is large enough to enable the reader to demodulate the backscattered signal correctly.

Conventional passive tag RFID systems have one antenna to serve as receiving antenna and backscattering antenna[16, 17]. A single antenna cannot be designed optimally to meet the above two conditions at the same time because the design requirements are different. Recently, Chen et al.[15] have reported a pioneer work describing a proposal for a dual-antenna structure (DAS) to be used in UHF RFID tags.

* Corresponding author:
rsfyath@yahoo.com (R. S. Fyath)
Published online at http://journal.sapub.org/ijea

One of the antennas is for receiving and designed to have the maximum power transfer to the tag chip, while the other is for backscattering and designed for the maximum differential backscattering. The concepts are verified experimentally at 915 MHz using two linearly tapered meander dipoles printed on the opposite sides of the substrate.

It is worth to mention here that the issue of antenna miniaturization was not discussed by the authors in[15]. The work reported in this paper uses the main concepts reported in[15] to design a miniaturized DAS for 5.8GHz RFID tags. The miniaturization is based on particle swarm optimization (PSO) technique which is applied for both conventional DAS and its fractal counterpart. The fractal geometry is introduced in the structure to achieve further miniaturization. In fact, the electrodynamical properties of fractal geometries have been extensively studied by several authors focusing on their multiband behavior and ability to operate as efficient small antennas. As a matter of fact, the use of fractal geometries for antenna design has been proven to be very effective in achieving miniaturized dimensions and an enhanced bandwidth, even though a reduction of the radiation efficiency at resonance frequencies takes place[18]. Fractal geometry which is suitable for antenna design is infinite and there must be better shape candidates among those geometries for antennas. Therefore, design and fabricating of fractal geometry is the premier topic of research of fractal antenna.

The design issues reported in this paper takes the bow-tie antenna (BTA) as a reference one. It is well known that BTAs are a planar form of ultra-wideband finite biconical antennas. It is a practical angle-dependent frequency independent antenna[19]. Because of its ultra-broadband, light weight, thin profile configurations, low cost, and easiness of fabrication, reliability and conformability, BTAs have been widely studied and used in engineering applications. Also, the simple geometries make it compatible to be connected to planar feeding system in an integrated architecture. In this paper, a modified Sierpinski gasket fractal geometry with ellipse generation is designed and introduced into the typical bow-tie antenna.

The goal of this paper is to introduce optimization based-approach for miniaturizing DAS for RFID tag systems. One of the main advantages of this approach is its ability to generate automatically the shape of the antenna according to both the geometric antenna parameters constraints and required optimization fitness function. The steps followed to design a miniaturized DAS are introduced and investigated in detail. The impedance matching and radiation characteristics of the optimized conventional and fractal BTA-based DASs are presented and discussed for 5.8GHz operation.

2. Concepts of Dual-Antenna Structure

In a conventional loaded antenna (such as RFID tag), the scattered field can be considered from either load-dependent component (associated with re-radiated power from the match-loaded antenna) or load-independent components (associated with scattering from the open- or short-circuited antenna)[20]. For minimum scattering antenna this power can be calculated from the antenna equivalent circuit of Fig. 1a (where $Z_a = R_a + jX_a$ is the antenna input impedance and Z_L is the antenna load). The load Z_L takes one of the following modes:

(i) Backscattering mode
- $Z_L = Z_{L1}$ corresponding to open-circuited load state.
- $Z_L = Z_{L2}$ corresponding to short-circuited load state.

(ii) Receiving mode
- $Z_L = Z_C$ corresponding to the complex input impedance of the chip.

The complex reflection coefficient at the load is given by

$$\Gamma(Z_L) = \frac{Z_L - Z_a^*}{Z_L + Z_a} \quad (1)$$

The ideal case of $Z_{L1} \to \infty$, $Z_{L2} = 0$ and $Z_C = Z_a^*$ (perfect matching), yields $\Gamma(Z_{L1}) = -1$, $\Gamma(Z_{L2}) = +1$, and $\Gamma(Z_C) = 0$. The difference of the two scattering levels, $\Delta \propto |\Gamma(Z_{L1}) - \Gamma(Z_{L2})|, = 2$.

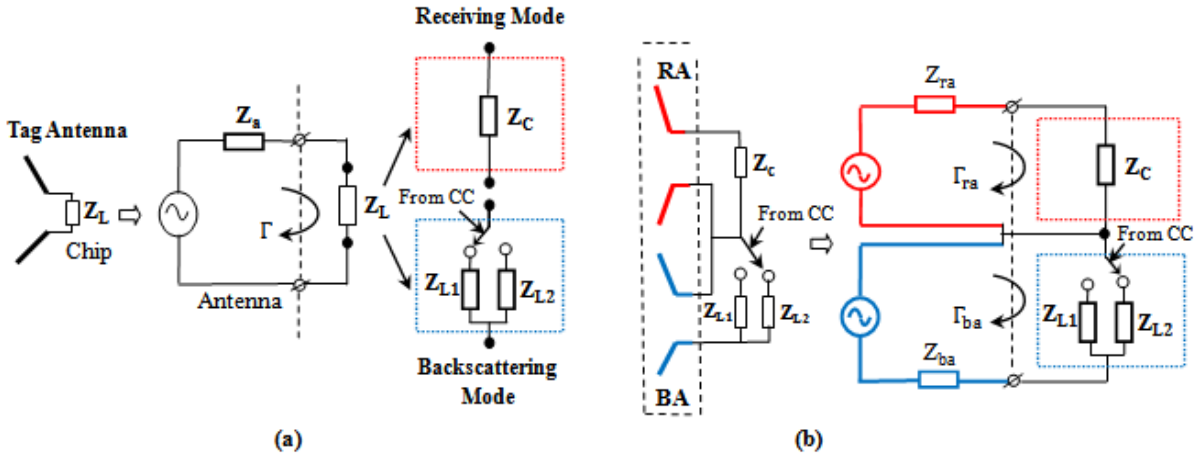

Figure 1. RFID tag and its equivalent circuit. **(a)** Conventional. **(b)** Dual-antenna structure (DAS). RA= Receiving Antenna, BA=Backscattering Antenna, CC= Control Circuit

Figure (1b) shows the configuration of the RFID DAS along with it's equivalent block diagram. The receiving input antenna impedance, Z_{ra} should be conjugate matched to the input impedance of the chip, Z_C (i.e., $Z_C = Z_{ra}^*$) to ensure maximum power transfer to the chip (i.e., the receiving antenna reflection coefficient $\Gamma_{ra}(Z_c)=0$). The backscattering antenna operates with two different load states, namely very high-impedance load Z_{L1} when the switch is OFF and very low-impedance load Z_{L2} when the switch is ON. The control circuit (CC) within the chip is responsible for switching the impedance states according to the data stored. The difference in the scattered field strength between the two states Δ is proportional to $|\Gamma_{ba}(Z_{L1})-\Gamma_{ba}(Z_{L2})|$, where Γ_{ba} is the backscattering reflection coefficient. The parameter Δ should be maximized to enable the reading antenna to simply differentiate between the high level and low level of the backscattered signals modulated in accordance with the data stored in the tag chip. This condition is best satisfied when $\Gamma_{ba}(Z_{L1}) = -\Gamma_{ba}(Z_{L2}) = \exp(j\theta)$ for any argument θ[15].

The condition $\Gamma_{ba}(Z_{L1}) = -\Gamma_{ba}(Z_{L2})$ reveals that

$$\frac{Z_{L1}-Z_{ba}^*}{Z_{L1}+Z_{ba}} = \frac{Z_{ba}^*-Z_{L2}}{Z_{L2}+Z_{ba}} \quad (2)$$

This yields

$$\frac{2Z_{ba}Z_{ba}^*}{Z_{L1}} - \left(1+\frac{Z_{L2}}{Z_{L1}}\right)(Z_{ba}-Z_{ba}^*) - 2Z_{L2} = 0 \quad (3)$$

Let

$$Z_{ba} = r_{ba} + jx_{ba} \quad (4a)$$
$$Z_{L1} = r_1 + jx_1 \quad (4b)$$
$$Z_{L2} = r_2 + jx_2 \quad (4c)$$

Then eqn. (3) can be split into two expressions

$$r_{ba}{}^2 + x_{ba}{}^2 + (x_1+x_2)x_{ba} - (r_1r_2 + x_1x_2) = 0 \quad (5a)$$
$$(r_1+r_2)x_{ba} + (r_1x_2 + r_2x_1) = 0 \quad (5b)$$

Equation (5b) can be rewritten as

$$x_{ba} = -\frac{r_1x_2+r_2x_1}{r_1+r_2} \quad (6)$$

which determines the required value of backscattering antenna reactance when load impedances are known. Substituting eqn. (6) into eqn. (5a) yields

$$r_{ba} = \left[(r_1r_2 + x_1x_2)\left(1+\frac{r_1x_2+r_2x_1}{(r_1+r_2)^2}\right)\right]^{1/2} \quad (7)$$

Equation (7) describes the dependence of backscattering antenna resistance on load parameters when $\Gamma_{ba}(Z_{L1}) = -\Gamma_{ba}(Z_{L2})$.

For ideal switching states (i.e., $x_1 = x_2 = 0$, $r_1 \to \infty$, and $r_2 = 0$), eqn. (7) gives $x_{ba} = 0$ and predicts a finite value for r_{ba}. Under this environment, $\Gamma_{ba}(Z_{L1}) = -1$ and $\Gamma_{ba}(Z_{L2}) = +1$ which offer the maximum allowable value of $\Delta = 2$.

3. Design of Bow-Tie Antenna

Figure 2 shows detailed design geometry of a BTA which will be used as a reference structure to optimize both the receiving and backscattering antennas for conventional and dual-antenna structure. Initially, the antenna is designed using a set of equations and then the results are fine-tuned using CST software to achieve the required resonance frequency.

The used design equations are[21]

$$f_r = \frac{v}{2\sqrt{\epsilon_e}\,S}\left(\frac{1.152}{R_t}\right) \quad (8a)$$

$$R_t = \frac{S}{2}\frac{(W_p+2\Delta l)+(W_c+2\Delta l)}{(W_p+2\Delta l)(L_p+2\Delta l)} \quad (8b)$$

$$\Delta l = h\frac{0.412(\epsilon_e+0.3)\left(\frac{W_i}{h}+0.262\right)}{(\epsilon_e-0.258)\left(\frac{W_i}{h}+0.813\right)} \quad (8c)$$

$$\epsilon_e = \left(\frac{\epsilon_r+1}{2}\right)+\left(\frac{\epsilon_r-1}{2}\right)\left(1+\frac{12h}{W_i}\right)^{-1/2} \quad (8d)$$

$$W_i = \left(\frac{W_p+W_c}{2}\right) \quad (8e)$$

where f_r is the resonance frequency and the substrate is characterized by three parameters h, ϵ_r and ϵ_e which denote its thickness, relative and effective permittivity, respectively. Other geometric parameters appeared in these equations are defined in Fig. 2.

The reference BTA is designed to resonate at 5.8 GHz using a substrate having h = 1.6 mm and $\epsilon_r = 4.3$ (FR4). The initial design starts with the assumption that each side of the BTA is approximated by an equilateral triangle (i.e., $S/2 \cong Wp$ and $Wp \gg Wc$). From antenna basic theory, the effective length of the antenna "S" should be approximately equal to $\lambda/2 = v/2f_r$ where λ is the resonance wavelength and v is the speed of light in free space.

The initial design takes $Wp = \lambda/4 = 12.93$ mm and $W_c = 0$. Equation (8d) predicts an effective permittivity ϵ_e of 3.48 (which is less than $\epsilon_r = 4.3$) and accordingly eqn. (8c) gives Δl=0.68 mm. Afterwards, the value of the geometric parameter S can be computed by combining eqns. (8a) and (8b) to get the following equation

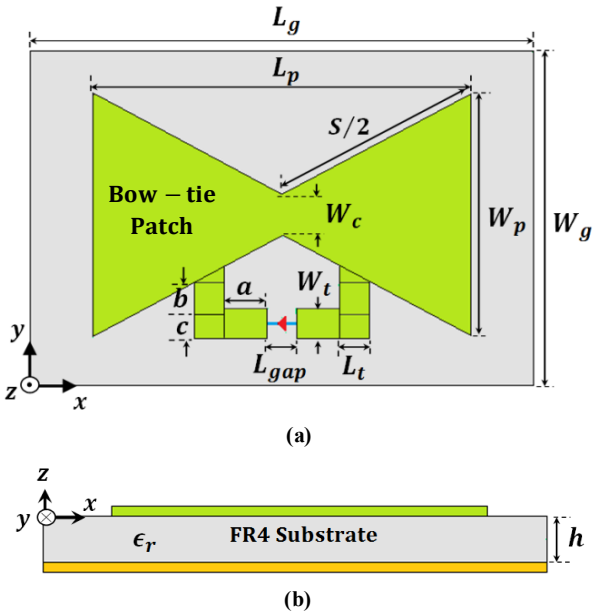

Figure 2. Geometry of the bow-tie patch including matching loop. **(a)** Front view. **(b)** Bottom view

$$q^2S^4 - (4pq\,\Delta l + p^2)\,S^2 + p^2(W_p - W_c)^2 + 4p^2\,\Delta l^2 = 0 \quad (9)$$

where

$$p = \frac{1.152c}{2\sqrt{\epsilon_e}\, f_r} \quad (10a)$$

$$q = \frac{(W_p + 2\,\Delta l) + (W_c + 2\,\Delta l)}{2(W_p + 2\,\Delta l)} \quad (10b)$$

In writing eqn. (9), we substitute eqn. (8b) into eqn. (8a) and use

$$L_p = \left[S^2 - (W_p - W_c)^2\right]^{1/2} \quad (11)$$

The solution of eqn. (9) is

$$S = \frac{1}{\sqrt{2}q}\left[m + (m^2 - 4q^2 n)^{1/2}\right]^{1/2} \quad (12)$$

where

$$m = 4pq\,\Delta l + p^2 \quad (13a)$$

$$n = p^2(W_p - W_c)^2 + 4p^2\,\Delta l^2 \quad (13a)$$

Equation (12) gives S = 27.10 mm.

Table 1 lists the initial values of the geometric parameters used to run the CST software. The antenna design is fine-tuned and the final design obtained after numerical CST simulation is listed in the same table. Note that f_r is shifted from 5.66 GHz (theoretical) in the initial design to 5.80 GHz (simulation) in the finalized design.

Table 1. Geometric parameters of the reference BTA at $f_r = 5.8$ GHz (λ=51.72 mm). $L_{gap} = L_t = W_t = 1$ mm

Parameter	Initial value		Final value	
	(λ)	(mm)	(λ)	(mm)
L_g	0.750	38.80	0.522	27.00
W_g	0.750	38.80	0.405	20.80
L_p	0.500	25.86	0.304	15.80
W_p	0.500	25.86	0.321	16.60
W_c	0.000	0.00	0.032	1.66
S	0.524	27.10	0.420	21.76
a	0.250	12.93	0.037	1.92
$b + c$	0.250	12.93	0.042	2.20

4. Design Optimization Approach

An optimal approach for exploiting miniaturization and matching properties of DAS for RFID tag systems is based on introducing dependent and independent geometric parameters. This to ensure more degrees of freedom for antenna design, avoid the generation of unrealizable structures, and prevent the occurrence of failure in optimization process. Accordingly, to comply with electrical and geometric constraints by properly defining the geometric parameters of the radiating antenna structure (bow-tie with matching loop), the design procedure can be considered as an optimization problem. In the following subsection, a detailed optimization design approach and the performances of the miniaturized single- and dual-antenna structures for RFID tags are presented.

Figure 3 illustrates the geometry of the proposed dual-bow-tie antenna with its matching loop. The structure consists of both receiving and backscattering antennas. The two antennas are printed on opposite sides of the structure and perpendicular with each other to reduce coupling between them.

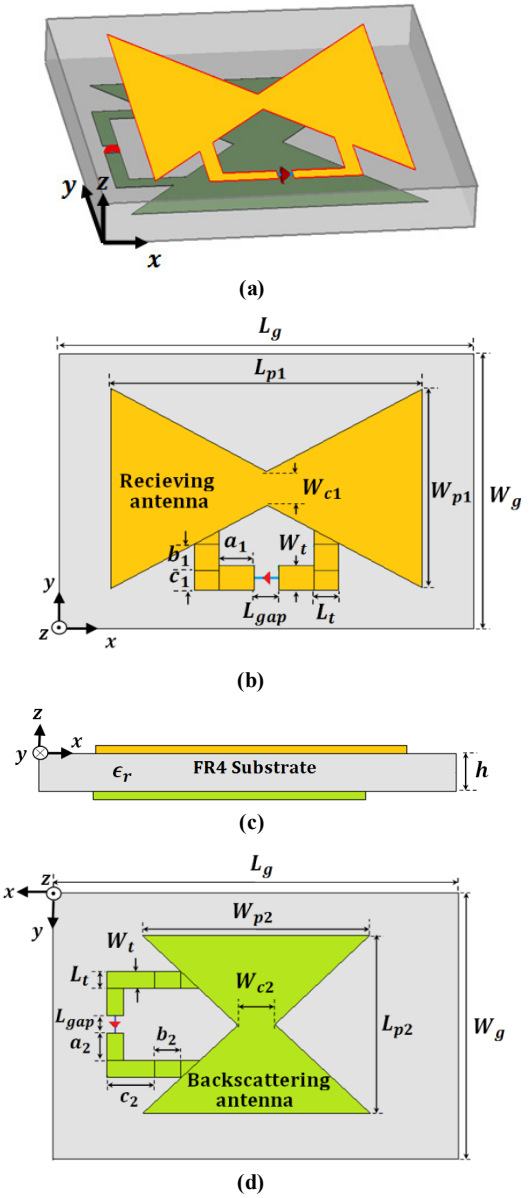

Figure 3. Proposed dual-antenna geometry. **(a)** 3D configuration. **(b)** Front side. **(c)** Bottom side. **(d)** Back side

4.1. Conventional Backscattering Antenna

In this subsection, the designs of miniaturized backscattering antennas (MBAs) for different desired real input impedances are presented. The main goal of this design is to investigate the dependence of the miniaturized area on the input antenna impedance. Different desired input impedances, $Z_a = Z_d$ (50, 100, 150, 200, 250 and 500Ω) are chosen for designing a backscattering antenna with miniaturized area. The geometry of the backscattering antenna is the same as that in Fig. 2, but with replacing its

front side by its back side (i.e., bow-tie patch printed in the back side substrate). Additional subscript 2 is added to the symbols to define bow-tie and matching loop geometry parameters for this antenna.

Eight antenna geometric parameters enter the optimization process, one is considered as independent parameter, ground length L_g, and the other seven are considered as dependent parameters. Equation (14) describes the relation among dependent and independent geometric parameters

$$W_g = K_{W_g} \times L_g \quad (14a)$$

$$L_{p2} = K_{L_{p2}} \times W_g \quad (14b)$$

$$W_{p2} = K_{W_{p2}} \times L_g \quad (14c)$$

$$W_{c2} = K_{W_{c2}} \times L_p \quad (14d)$$

$$a_2 = K_{a_2} \times (0.5W_{p2} - 1.5) \quad (14e)$$

$$b_2 = K_{b2} \times \left(0.5L_{p2} - \frac{L_{p2} - W_{c2}}{W_{p2}}\right) + 0.5W_{c2} + \left(0.5 + L_2 \frac{L_{p2} - W_{c2}}{W_{p2}}\right) \quad (14f)$$

$$c_2 = 0.5\, K_{c_2} \times (L_g - L_{p2}) \quad (14g)$$

In eqns. (14a)-(14d), K_{W_g}, $K_{L_{p2}}$, $K_{W_{p2}}$, and $K_{W_{c2}}$, represent, scaling parameters for generation the corresponding parameters, ground length L_g, patch length L_{p2}, patch width W_{p2}, and W_{c2}, respectively. Whereas, in eqns. (14e)-(14g), K_{a_2}, K_{b_2}, and K_{c_2} denote the scaling parameters that responsible for matching loop parameters generation a_2, b_2, and c_2, respectively.

The following optimization fitness function is used to miniaturize this antenna for different values of Z_d.

Minimize the fitness function

$$Fit(x) = \Gamma_{obj} + A_{obj} \quad (15a)$$

where

$$\Gamma_{obj} = (\Gamma_{ba} - \Gamma_d) \cdot u(\Gamma_{ba} - \Gamma_d) \quad (15b)$$

$$A_{obj} = \left(\frac{A}{A_{ref}} - 1\right) \quad (15c)$$

$$Subject\ to: \quad A < A_{ref}$$

$$and\ the\ constraints: \quad x_i^l \le x_i \le x_i^u, \quad i = 1,2,\ldots N$$

Note that the optimization fitness function, eqn. (15a) consists of two objective functions Γ_{obj} and A_{obj} which are related to complex return loss and antenna area, respectively. In eqn. (15b), Γ_{ba} and Γ_d represent, respectively, the actual and desired values of backscattering reflection coefficient at resonance frequency, and u is the unit step function. In eqns. (15b) and (15c), A_{ref} and A represent, respectively, the area of the reference and the optimized antennas. Also, x_i^l and x_i^u are the lower and upper bounds on the N design variables, respectively.

The PSO algorithm adopted here is a basic one follows closely with that in Ref.[22]. The number of PSO particles required to perform the optimization are 24 particles, three for each one of the eight parameters that entered the optimization. A stop criterion is chosen such that 60 PSO iterations are reached or the fitness function remains unchanged with less than 2% error for at least 20 successive iterations. The constraints used in the optimization process for the geometric parameters of the backscattering antennas are listed in Table 2.

Table 2. Ranges of the design parameters for the MBAs

Parameter	Range
L_g (mm)	8.00 ~ 24.00
K_{Wg}	0.75 ~ 1.25
K_{Lp2}	0.40 ~ 0.90
K_{Wp2}	0.40 ~ 0.90
K_{Wc2}	0.05 ~ 0.20
K_{a2}	0.10 ~ 0.90
K_{b2}	0.10 ~ 0.90
K_{c2}	0.10 ~ 0.90

Table 3. Performance of the conventional backscattering antenna for different values of desired antenna input impedance Z_d (50, 100, 150, 200, 250 and 500Ω) at f_r = 5.8 GHz

Parameter	Antenna Performance						
	Reference BTA	Miniaturized BTAs					
Z_d(Ω)	50+j0	50+j0	100+j0	150+j0	200+j0	250+j0	500+j0
Z_{ba}(Ω)	55.9-j1.7	49.0-j1.3	103.0+j11.0	148.5+j6.2	203.6-j0.8	253.2+j5.9	469.2-j25.0
Γ_{ba} (dB)	-25.43	-35.67	-25.11	-27.26	-40.43	-35.87	-33.08
G (dB)	-0.82	2.66	1.55	-3.27	2.39	-0.48	0.93
η (%)	30.87	61.07	44.73	21.78	58.16	30.57	41.00
BW (GHz)	362	725	427	290	616	342	378
L_g (mm)	27.00	16.69	15.29	11.97	17.50	14.21	14.96
W_g (mm)	20.79	9.57	11.35	8.61	9.03	7.23	9.76
A (mm^2)	561.33	159.72	173.54	103.06	158.02	102.73	146.00
A/A_{ref}	1.00	0.28	0.31	0.18	0.28	0.18	0.26

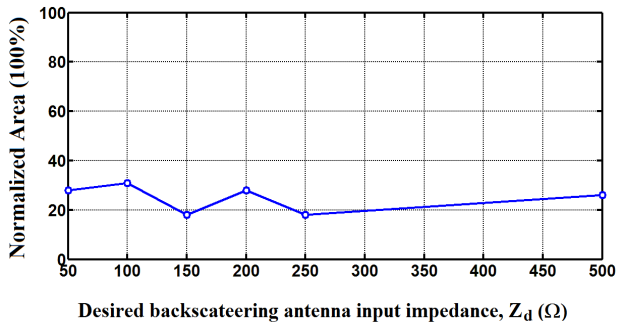

Figure 4. Normalized area versus the desired backscattering input impedance, Z_d

Table 3 lists the miniaturized area and the performance parameters of the backscattering antenna for different values of desired input resistance. Figure 4 shows the relation between the normalized area and the desired input impedance Z_d. One can see from Table 3 and Fig. 4 that a normalized area of 18%-28% is achieved for these antennas, i.e., antenna areas of 102 - 173 mm^2, for. $Z_d = 50\text{-}500\,\Omega$. Also, It seen from Table 3 that the miniaturized BA for $Z_d = 50\Omega$ gives good performance (gain of 2.66 dB, efficiency $\eta = 61.07\%$ and bandwidth BW=725 MHz) compared with other antennas of $Z_d \neq 50\Omega$. Thus, $Z_d = 50\Omega$ is used as the desired real-valued input impedance for the backscattering antenna during the optimization of the DAS in the following subsections.

Figure 5 depicts the return loss and input impedance of the miniaturized backscattering antenna for $Z_a = Z_d = 50\ \Omega$. One can conclude from this figure that complex return loss of -38.44 dB with input resistance and reactance of 49.27Ω and -0.94 Ω, respectively, at 5.8 GHz resonance frequency are achieved. The 3D radiation pattern of this antenna is shown in Fig. 6. It is noticed from this figure that maximum radiation pattern is in the broadside direction of the patch and minimum or approximately no radiation behind the backside (ground plane).

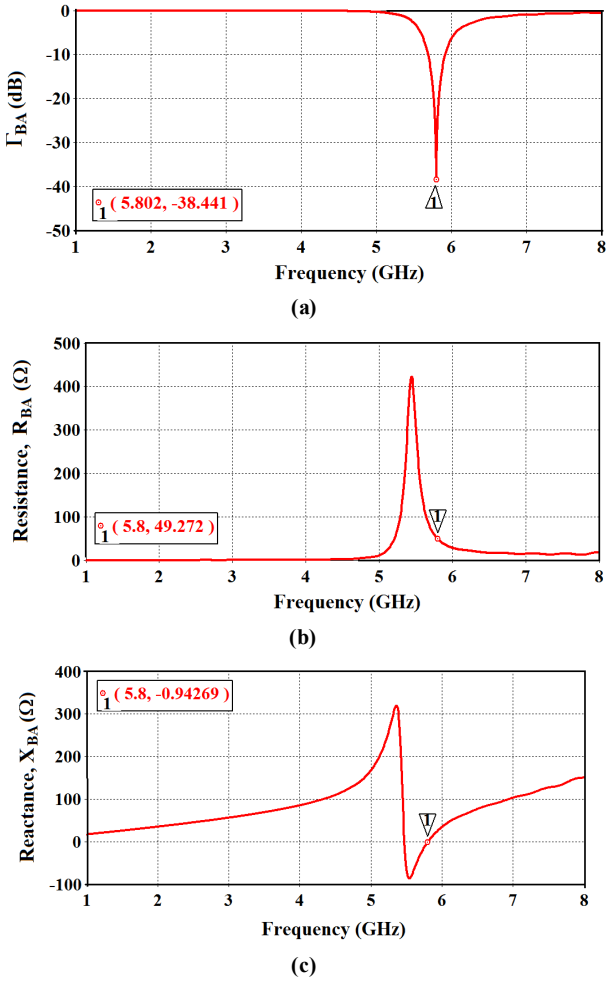

Figure 5. Return loss **(a),** input, resistance **(b),** and input reactance **(c)** of the miniaturized BA with $Z_a = 50\ \Omega$

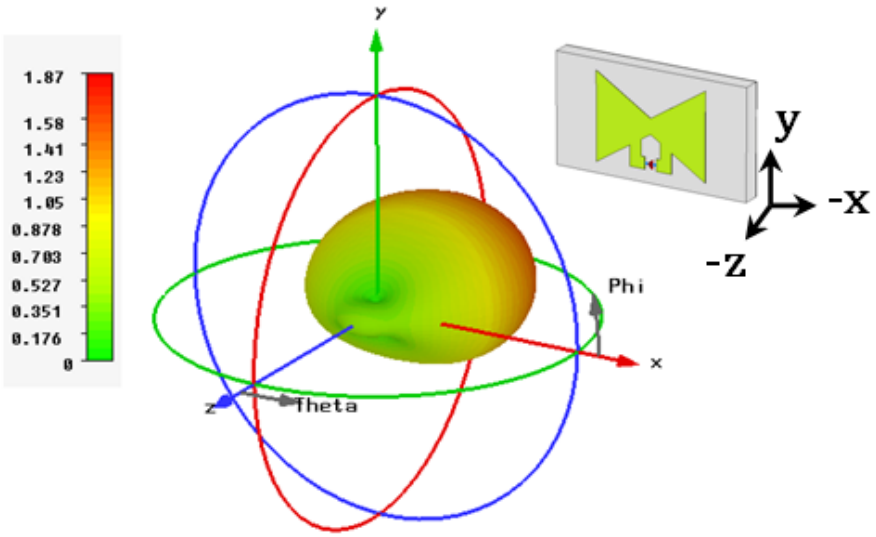

Figure 6. 3D radiation pattern (gain) of the miniaturized BA with $Z_a = 50\ \Omega$. Note that (-z and –x) coordinates are used here to see clearly the radiation

4.2. Conventional Receiving Antenna

In this subsection, the receiving antenna is optimized in the same manner that mentioned in previous subsection, but for conjugate impedance matching $Z_a = Z_c^*$. The structure of this antenna is the same as that of Fig. 2. An additional subscript 1 is added to the symbols of geometric parameters of the bow-tie patch-shape and matching loop structure. The optimization fitness function, eqn. (15a), is used for miniaturizing this antenna with the receiving antenna return loss Γ_{ra} defined in eqn. (1) for $Z_L = Z_C$. The antenna is optimized for $Z_C = (10 - j160)\ \Omega$ at resonance frequency $f_r = 5.8GHz$. The used geometric parameters, ranges of constraints, and number of particles are as in the previous subsection.

The return loss and the corresponding input resistance and reactance of the miniaturized receiving antenna (MRA) are shown in Fig. 7. It is shown from this figure that good conjugate matching with complex load Z_C=(10-j160) Ω is achieved at f_r=5.8GHz. Return loss less than -39 dB and input impedance 10.10+j159.79 Ω at 5.8 GHz are obtained. The 3D radiation pattern of MRA is shown in Fig. 8. Note that more radiation is in the front of the patch and less radiation in its back side.

Table 4 lists the optimized geometric parameters for the receiving, backscattering, and the reference antennas. The corresponding performance parameters are given in Table 5. The following findings can be drawn from these two tables:

i) Return loss less than -25 dB at the resonance frequency 5.8 GHz is achieved for all antennas.

ii) Miniaturized backscattering antenna has the greatest gain and bandwidth (2.66 dB and 720 MHz) while the receiving antenna has the lowest gain and bandwidth (-3.99 dB and 240 MHz).

iii) The receiving antenna offers higher reduction of area (1- A/A_{ref}) ,(81%) compared with backscattering antenna (71%)

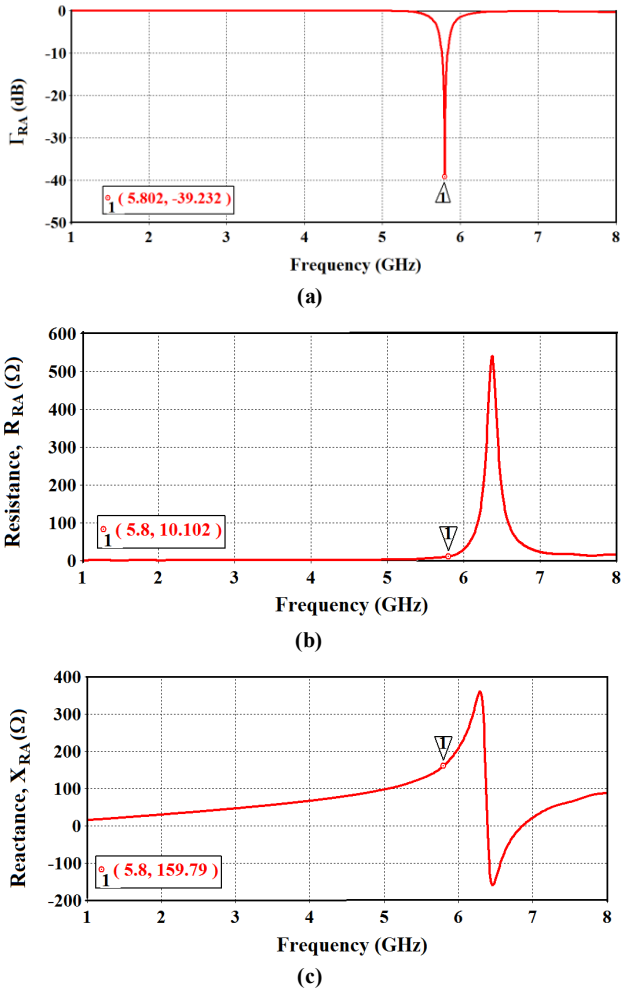

Figure 7. Return loss **(a),** input resistance **(b),** and input reactance **(c)** of the miniaturized RA for Z_c=(10-j160) Ω

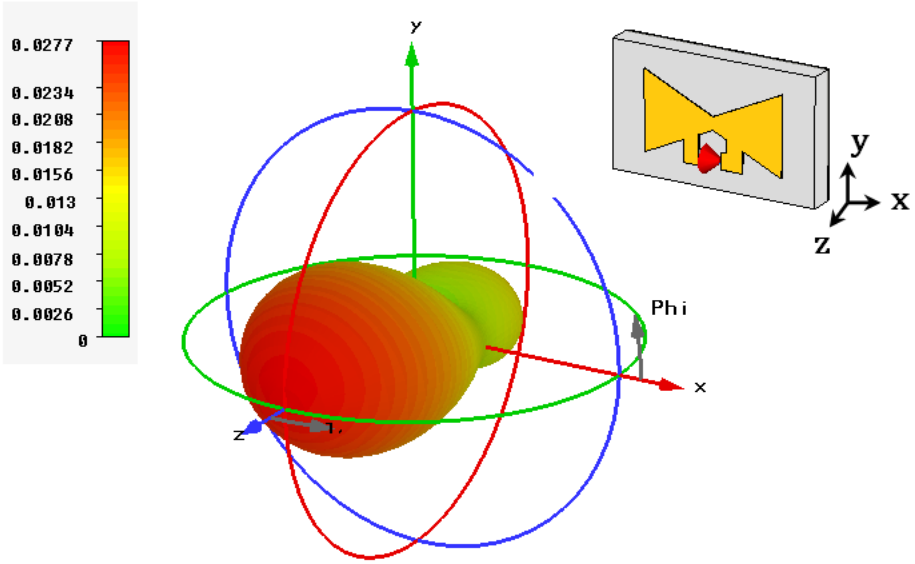

Figure 8. 3D radiation pattern (gain) of the MRA for Z_c=(10-j160) Ω

Table 4. Geometric parameters of the miniaturized receiving and backscattering conventional antennas at f_r = 5.8 GHz. Rsesults corresponding to the reference antenna are also included for comparision purposes

Parameter	Value (mm)		
	Reference BTA Front view Back view BA (ported)	Miniaturized BA Front view Back view BA (ported)	Miniaturized RA Front view Back view RA (ported)
L_g	27.00	16.69	12.70
W_g	20.79	9.22	7.63
L_p	15.79	9.64	8.64
W_p	16.63	7.37	4.88
W_c	1.66	1.29	0.78
a	1.92	1.00	0.28
b+c	1.05	1.62	1.10
h	1.60	1.60	1.60

Legend: RA=Receiving Antenna; **BA**=Backscattering Antenna

Table 5. Performance parameters of miniaturized receiving and backscattering conventional antennas at f_r = 5.8 GHz. Rsesults corresponding to the reference antenna are also included for comparision purposes

Antenna Parameter	Value		
	Reference BTA Front view Back view BA (ported)	Miniaturized BA Front view Back view BA (ported)	Miniaturized RA Front view Back view RA (ported)
$Z_d(\Omega)$	BA: 50+j0 RA: 10+j160	BA: 50+j0 RA: 10+j160	BA: 50+j0 RA: 10+j160
$Z_a(\Omega)$	BA: 49.47-j0.94	BA: 49.47-j0.94	RA: 10.10+j159.79
Γ (dB)	-25.86	-35.67	-39.23
G (dB)	-0.57	2.66	-3.98
η (%)	32.60	61.07	15.92
BW (GHz)	0.35	0.72	0.24
f_L(GHz)	5.65	5.52	5.68
f_H (GHz)	6.00	6.24	5.92
A (mm^2)	561.60	160.32	110.5
A/A_{ref}	-	0.28	0.19

4.3. Dual-Antenna Structure

In the previous subsections, the performance of conventional antenna structure for receiving and backscattering sides are designed and investigated in detail. In this subsection, the DAS presented in Fig. 3 is designed and investigated. In this design, the proposed antenna is printed on a 1.6-mm thick FR4 substrate of varying size $(L_g) \times (W_g) \times 1.6\ (h)$ mm3 comprising a radiating portions (bow-tie shape and matching loop) at both of its side. The dimensions of the radiating portion and matching loop of the receiving antenna are denoted by $(Lp1 \times Wp1)$ and $a_1 \times (b_1 + c_1)$, respectively. For the scattering antenna, the dimensions of the radiation portion and matching loop are denoted by $(Lp_2 \times Wp_2)$ and $a_2 \times (b_2 + c_2)$, respectively.

The fitness function used to miniaturize this antenna is the same as that in eqn. (15), but the return loss objective function consists of two terms rather than one term. Thus, eqn. (15) is rewritten as

Minimize the fitness function

$$Fit(x) = \Gamma_{obj\,1} + \Gamma_{obj\,2} + A_{obj} \quad (16a)$$

where

$$\Gamma_{obj\,1} = (\Gamma_{ra} - \Gamma_d) \cdot u(\Gamma_{ra} - \Gamma_d) \quad (16b)$$

$$\Gamma_{obj\,2} = (\Gamma_{ba} - \Gamma_d) \cdot u(\Gamma_{ba} - \Gamma_d) \quad (16c)$$

$$A_{obj} = \left(\frac{A}{A_{ref}} - 1\right) \quad (16d)$$

Subject to: $A < A_{ref}$

and the constraints: $x_i^l \le x_i \le x_i^u, \quad i = 1,2,\ldots N$

where Γ_{ba} and Γ_{ra} represent the complex return loss of backscattering and receiving antennas at the resonance frequency f_r, respectively. The goal of this fitness function is to miniaturize the overall area (Lg x Wg) of this DAS subject to keeping both the return losses Γ_{ba} and Γ_{ra} below the desired value Γ_d = -15 dB at the required resonance frequency f_r.

The geometric parameters enter the optimization process are fourteen, two for the common ground, L_g and W_g, and six for the receiving (backscattering) bow-tie shapes, Lp_1 (Lp_2), Wp_1 (Wp_2) and Wc_1 (Wc_2), and six for matching loop geometries a_1 (a_2), b_1 (b_2) and c_1 (c_2). The number of particles used to optimize this antenna is 42, three for each of the 14 geometric parameters that enter the optimization process.

5. Performance of the Dual-Antenna Structure

The proposed DAS is optimized to operate as receiving and backscattering antennas at the center frequency 5.8 GHz. The receiving antenna is to be conjugate matched to Z_C=(10-j160) Ω while the backscattering antenna having a 50Ω input impedance. In this section, the performance of this proposed antenna is presented and discussed for three cases:

Case 1: Both RA and BA are connected to a 50Ω-port or both antennas are under test (AUT).

Case 2: The RA is AUT and BA is connected to an open- or a short-circuited load.

Case 3: The BA is AUT and the RA is connected to a conjugate matched load.

5.1. Performance of RA When BA Being Open- or Short-Circuited (Case 2)

This subsection addresses the performance of the receiving antenna when the backscattering antenna being short- or open- circuited. Before doing this, the isolation coupling between RA and BA must be studied first since it's the most factors affecting the antenna performance. Figure 9 shows the isolation coefficient response for the proposed DAS. A coupling less than -17dB is obtained for frequencies less than 6 GHz, with less than -20 dB at 5.8 GHz. Thus, due to such low coupling, the receiving antenna is unaffected by shortening or opening the backscattering antenna. Also, the backscattering antenna is not affected by introducing the matching receiving antenna. Therefore, it is a good result to resume the simulation and address the performance of the proposed antenna.

Figure 10 shows the return loss and real and imaginary parts of the input impedance against frequency. It is seen from this figure that when the backscattering antenna is short circuited (BA_SC) or open circuited (BA_OC), nearly no changes occur in the return loss and input impedance of the receiving antenna beyond 5.8 GHz. In contrast, above 5.8 GHz, changes in return loss and impedance occur for the BA_SC while no changes in performance are obtained for the BA_OC. In addition, minimum changes are found for the imaginary part of input impedance of RA at 5.8 GHz for both cases, BA_SC or BA_O.C. Whereas more variation occur for the real part of input impedance of the RA at 5.8 GHz, +2.66 Ω and -3.80 Ω with respect to 10 Ω, real part of the load Z_C=(10-j160) Ω.

Figures 11(a) and 11(b) show the 3D gain pattern of the receiving and backscattering antennas, respectively. One can noticed from this figure that both antennas radiate in the front side of the dual-antenna structure

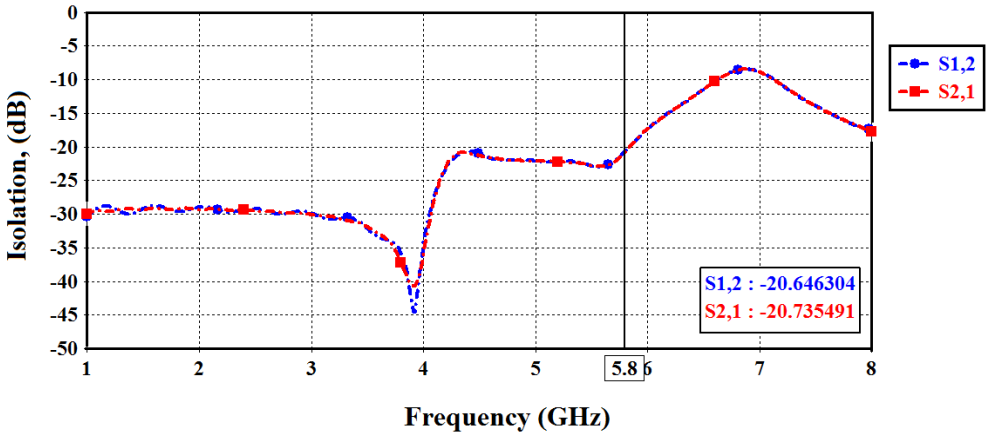

Figure 9. Isolation between receiving and backscattering antennas

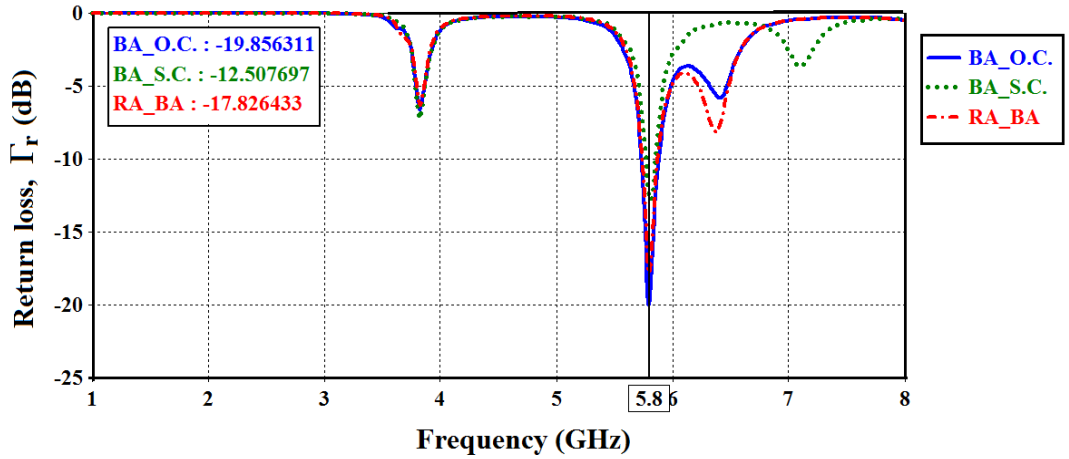

(a)

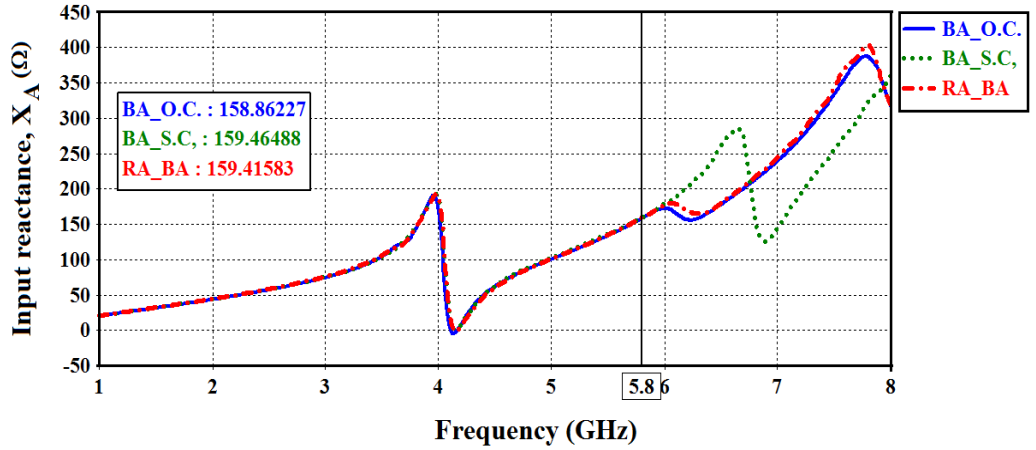

(b)

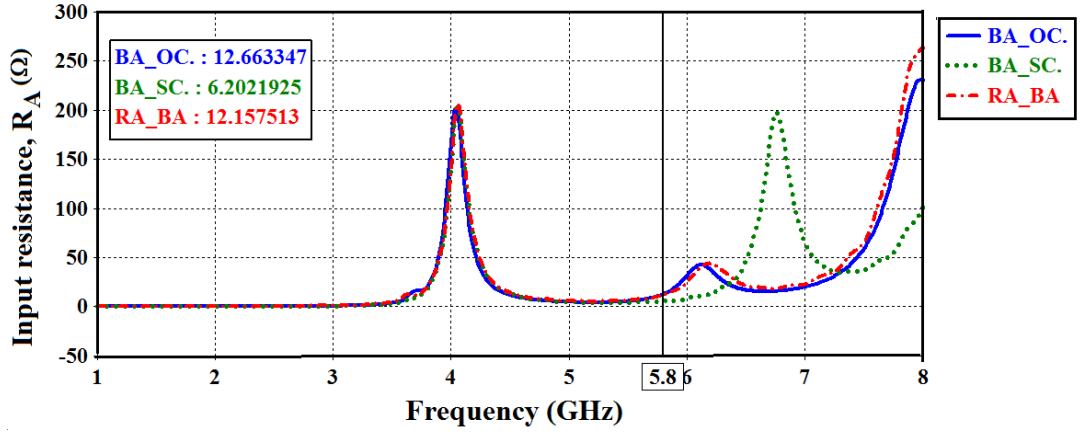

(c)

Figure 10. Return loss (a), input resistance (b), and input reactance (c) of the DAS when BA is open circuited (BA_OC) or short circuited (BA_SC), and when RA and BA are ported (RA_BA). Z_{ba}=50 Ω, and Z_{ra}= (10+j160) Ω

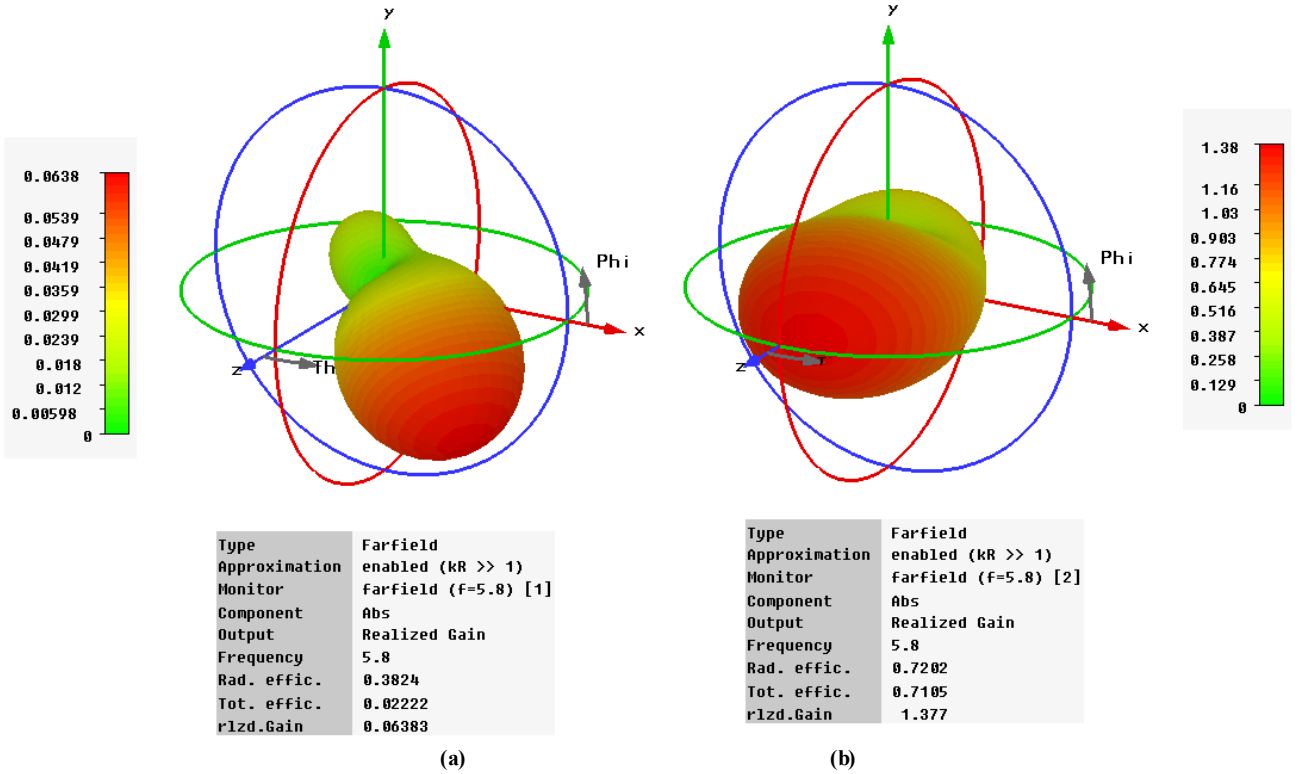

(a) (b)

Figure 11. 3D radiation pattern (gain) of the dual-antenna structure at 5.8 GHz when both RA and BA are under test. **(a)** RA. **(b)** BA

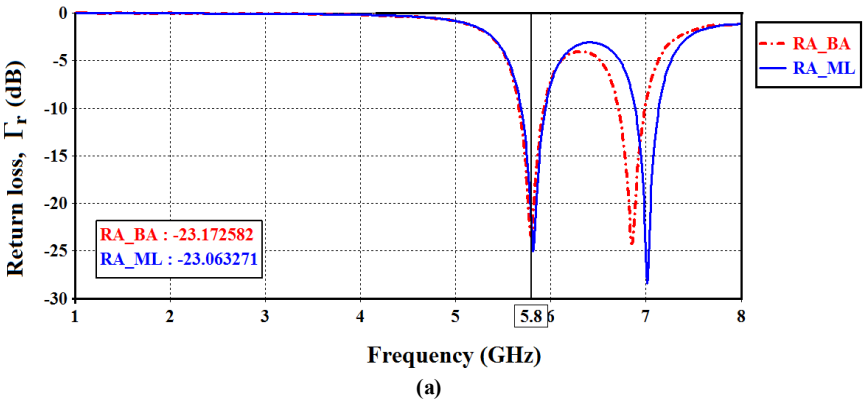

(a)

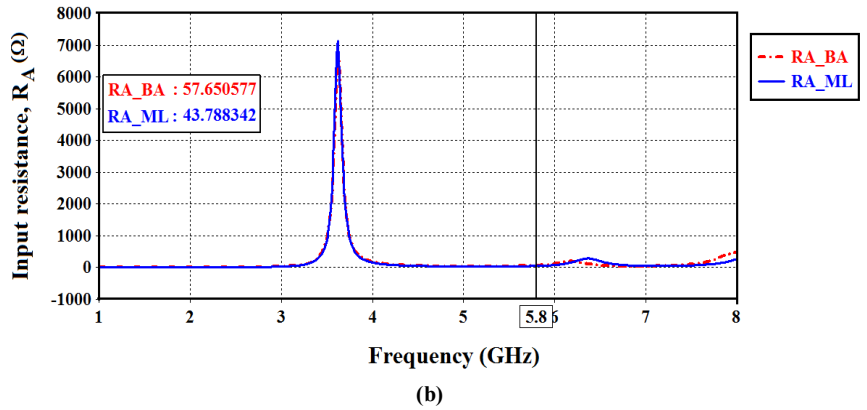

(b)

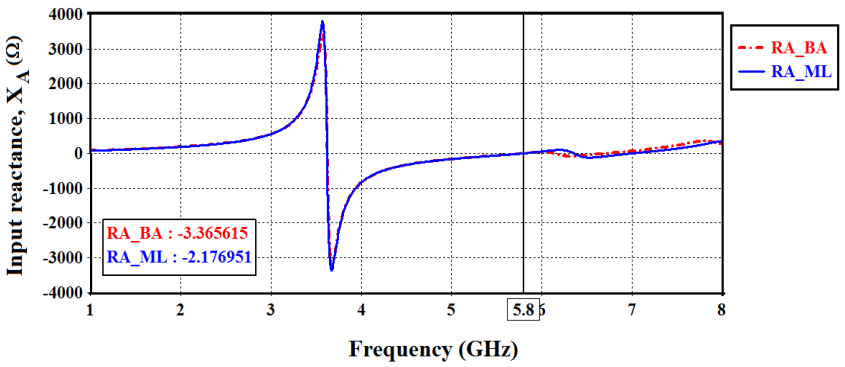

(c)

Figure 12. Return loss (a), input resistance (b), and input reactance (c) of the dual-antenna structure when RA is matched load (RA_ML), and when RA and BA are ported (RA_BA). Z_{ba}= 50 Ω and Z_{ra}= (10+j160) Ω

5.2. Performance of BA when RA Being Conjugate Matched (Case 3)

In this subsection, the performance of the backscattering antenna is investigated when the receiving antenna is matched to the load Z_C=(10-j160) Ω. Figure 12 shows the complex return loss and input impedance of the backscattering antenna which is AUT and the receiving antenna is connected to a matched load (case 3).

Investigating this figure reveals that the return loss and input impedance of the backscattering antenna are not affected by connecting a matched load to the receiving antenna. Table 6 lists a summary of the antenna performance for the aforementioned two cases beside case 1 (both antennas, RA and BA are AUT).

6. Dual-Fractal Antenna Structure

6.1. Modified Sierpinski Fractal Geometry

A fractal BTA (FBTA) is introduced here to miniaturize further the DAS for RFID tag applications at 5.8 GHz. The fractal geometry is embedded in both receiving and backscattering antennas. Figure (13) shows the first three fractal orders of the proposed FBTA. The fractal geometry used here is an extended version of the modified Sierpinski gasket adopted in[23]. The extension is based on ellipse fractal finger print rather than circle that used in[23]. The reason behind this modification is that the ellipse structure is characterized by higher degree of freedom which is required to enhance the filling factor of the fractal antenna and therefore more miniaturization will be achieved. The first -order fractal geometry shown in Fig. (13b) is constructed by subtracting a central ellipse I with radii α_1 and β_1 of 1/3-scaled of patch width (Wp) and halved-value patch length (Lp) of the main triangular shape. Three equal ellipses 1, 2, and 3, each one being (1/3) of the size of the ellipse I and placed at (Lp/16, Wp/2), (Lp/8, ±Wp/4), respectively, are subtracted from first fractal order geometry to produce second-order fractal, Fig. (13c). One can iterate the same subtraction procedure to generate a third-order structure by subtracting nine equal ellipses, each one being (1/3) of the size of the ellipses 1, 2 or 3, Fig. (13d). Equation (17) describes the geometrical parameters generation and their dependence on BTA parameters

$$\alpha_1 = W_p/3, \quad \alpha_{n+1}/\alpha_n = 1/3 \tag{17a}$$

$$\beta_1 = L_p/6, \quad \frac{\beta_{n+1}}{\beta_n} = 1/3 \tag{17b}$$

$$h_1 = 0, \quad h_2 = L_p/16, h_3 = 3L_p/32, \quad h_4 = L_p/4 \tag{17c}$$

$$g_1 = W_p/8, \quad g_{n+1}/g_n = 2 \tag{17d}$$

It is clear from Fig. (13b) and eqn. (17) that the first-order fractal consists of two symmetrical main ellipses lying in the centers of the two-sided of the bow-tie patch and with radii α_1 and β_1 of one-third and one-sixth of patch width Wp and patch length Lp, respectively. In the same manner, the second-order fractal is generated by subtracting six ellipses located at distances g_2, h_2 and $2h_2$ with respect to Wp and Lp, respectively, each one of one-third of the main ellipse, from the first-order fractal as shown in Fig. (13c). The third-order fractal is generated in the same procedure as shown in Fig. (13d).

In this work, a 3rd-order FBTA is miniaturized at 5.8 GHz to maximize the feeding power to the IC tag connected to the receiving antenna (conjugate matching with a chip having an input impedance of $10-j160\,\Omega$ and to make the input impedance of the backscattering antenna pure real (50Ω) for maximum backscattered field difference.

Table 7. Geometric parameters of the miniaturized receiving and backscattering fractal antennas at f_r = 5.8 GHz

Parameter	Value (mm)	
	RA	BA
L_g	13.93	13.93
W_g	13.23	13.23
L_p	8.64	11.46
W_p	9.05	10.00
W_c	1.88	0.52
a	0.05	0.92
$b+c$	2.50	2.04
h	1.60	1.60

Table 6. Performance parameters of the dual-antenna geometry at f_r = 5.8 GHz for the three operating cases

Parameters	RA (ported) BA (ported)	RA (ported) BA (open circuited)	RA (ported) BA (short circuited)	RA (matched) BA (ported)
Cases	**Case 1**	**Case 2**		**Case 3**
Z_d (Ω)	**BA:** 50+j0 **RA:** 10+j160	**BA:** 50+j0 **RA:** 10+j160	**BA:** 50+j0 **RA:** 10+j160	**BA:** 50+j0 **RA:** 10+j160
Z_a(Ω)	**BA:** 50+j0 **RA:** 12.16+j159.2	**RA:** 12.66+j158.86	**RA:** 6.20+j159.46	**BA:** 43.78-j2.17
$f_r(GHz)$	**BA:** 5.80 **RA:** 5.79	**RA:** 5.80	**RA:** 5.81	**BA:** 5.81
Γ (dB)	**RA:** -19.58 **BA:** -21.94	**RA:** -17.82	**RA:** -12.60	**BA:** -22.83
G (dB)	**RA:** 0.41 **BA:** 1.45	**RA:** 1.56	**RA:** 0.29	**BA:** 1.00
η (%)	**RA:** 38.24 **BA:** 72.02	**RA:** 62.54	**RA:** 34.60	**BA:** 56.21
BW (GHz)	**RA:** 0.95 **BA:** 0.55	**RA:** 0.93	**RA:** 0.32	**BA:** 1.96
L_g (mm)	24.00	24.00	24.00	24.00
W_g (mm)	12.00	12.00	12.00	12.00
A (mm^2)	288.00	288.00	288.00	288.00
A/A_{ref}	0.51	0.51	0.51	0.51

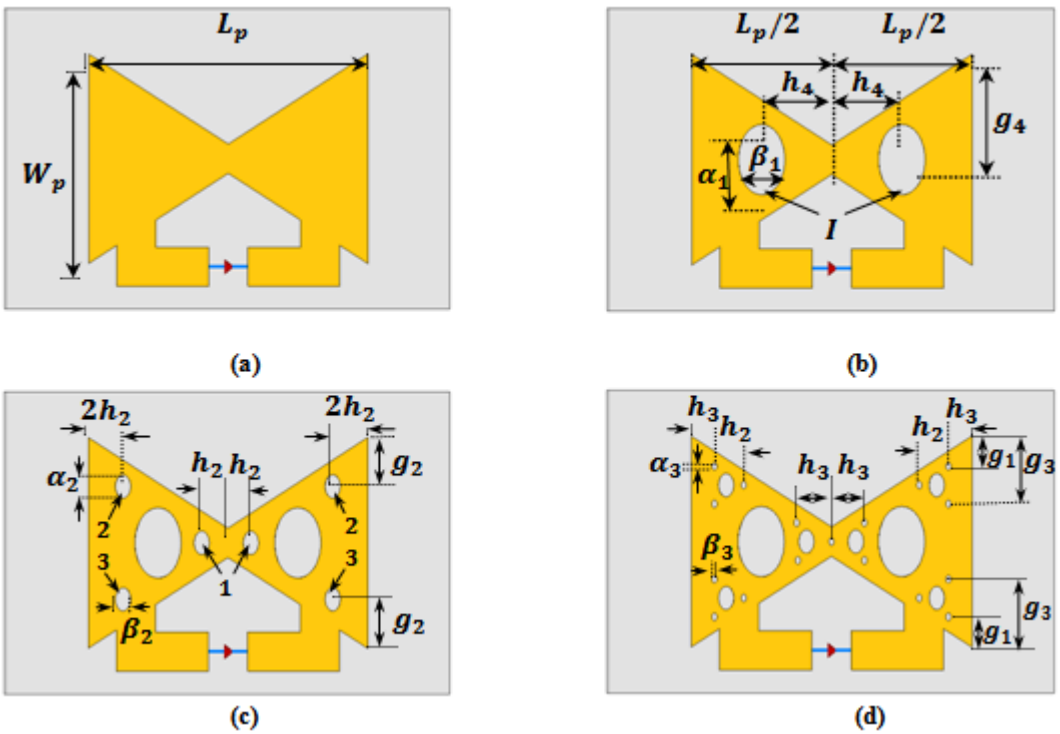

Figure 13. Front side of the dual-antenna structure with Sierpinski fractal bow-tie geometry and ellipse generation. **(a)** Reference BTA. **(b)** First-order FBTA. **(c)** Second-order FBTA. **(d)** Third-order FBTA

6.2. Performance of a 3rd-order FBTA

The optimization fitness function described by eqn. (16), is used here with 14 geometric parameters whose ranges are given in Table 4. Tables 7 and 8 list the antenna geometric and performance parameters for the 3rd-order FBTA. Investigating Tables 7, 8, and 5 reveals the following findings which are listed in Table 9.

(i) Area reductions of 68% and 49% are achieved by the 3rd-oredr fractal and conventional BTA for DAS, respectively, with respect to single-structure reference BA.

(ii) Bandwidth of (0.95 and 0.55 GHz) and (0.24 and 0.95 GHz) are obtained with the receiving and backscattering antennas by the fractal and non-fractal BTA, respectively.

Figure 14(a) and 14(b) show the isolation between receiving and backscattering antennas and the return losses of them. It is seen that more than 20 dB of isolation is achieved for frequencies less than 6.4 GHz, thus, good performance will be achieved for different operating conditions (cases 1-3). In Fig. 14(b), good matching of -12.63 and -17.07 dB are satisfied for the receiving and backscattering antennas at 5.8 GHz, respectively. Figures 15(a) and (b) depicts the resistance and reactance characteristics of the backscattering antenna when the receiving antenna is matched to a load of impedance 10-j160Ω. It is seen from this figure that a resistance of more than 60Ω and reactance less than -6Ω is achieved when the receiving antenna is ported to 50Ω or conjugate matched to the load. Figures 16(a) and (b) show the resistance and reactance of a receiving antenna when the backscattering antenna is connected to an open- or a short circuited load. Note that resistance between 15.90 Ω and 21.20 Ω, and reactance between 157.22 Ω and 161.26 Ω are obtained for the receiving antenna when the backscattering antenna is open- or short-circuited. Thus, good matching properties are achieved for both receiving and backscattering antennas irrespective of connecting load to a receiving antenna or making backscattering antenna short or open circuited.

Table 8. Performance parameters of the dual-fractal antenna geometry at f_r = 5.8 GHz. Both antennas RA and BA are excited by 50 Ω port

Parameters	Antenna Performance	
	RA	BA
Z_d (Ω)	10+j160	50
Z_a(Ω)	15.90+j161.27	66.18+j2.06
Γ (*dB*)	-12.63	-17.07
G (*dB*)	-0.84	1.50
η (%)	43.90	80.61
BW (*GHz*)	0.24	0.95
A (mm^2)	184.30	184.30
A/A$_{ref}$	0.32	0.32

Table 9. Performance of the miniaturized and reference antennas

Antenna Type		1-A/A$_{ref}$ (%)	G (*dB*)	η (%)	BW (*MHz*)
Reference BTA		-	-0.82	30.87	362
Dual-FBTA	RA	68	0.41	38.24	950
	BA		1.45	72.02	550
Dual-BTA	RA	49	-0.84	43.90	240
	BA		1.5	80.61	950

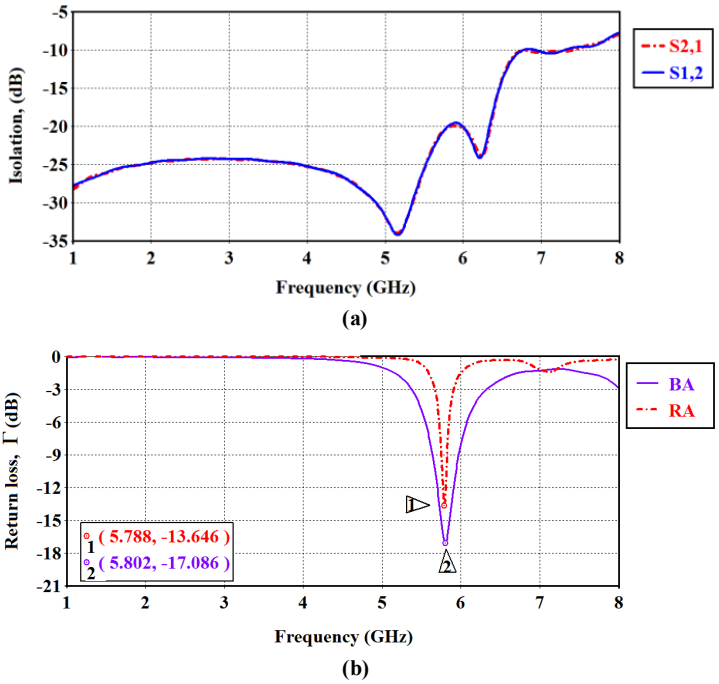

Figure 14. Isolation between the receiving and backscattering antennas **(a)** and return loss **(b)** of the fractal bow-tie antenna

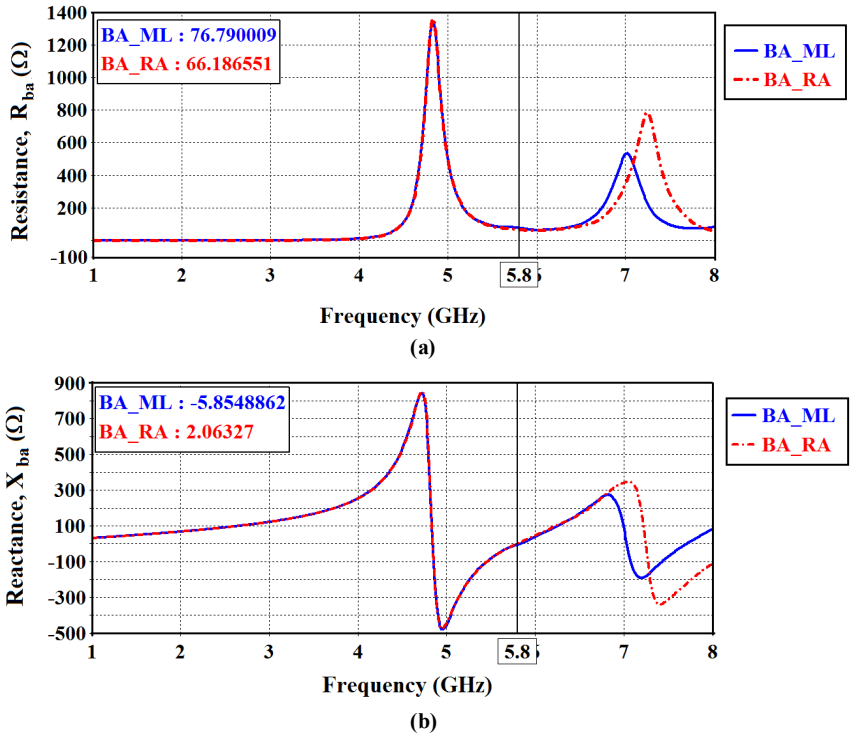

Figure 15. Input resistance (a) and input reactance (b) of the dual-fractal antenna structure when RA is matched load (RA_ML) and when RA and BA are ported (RA_BA). Z_{ba}=50 Ω and Z_{ra}= (10+j160) Ω

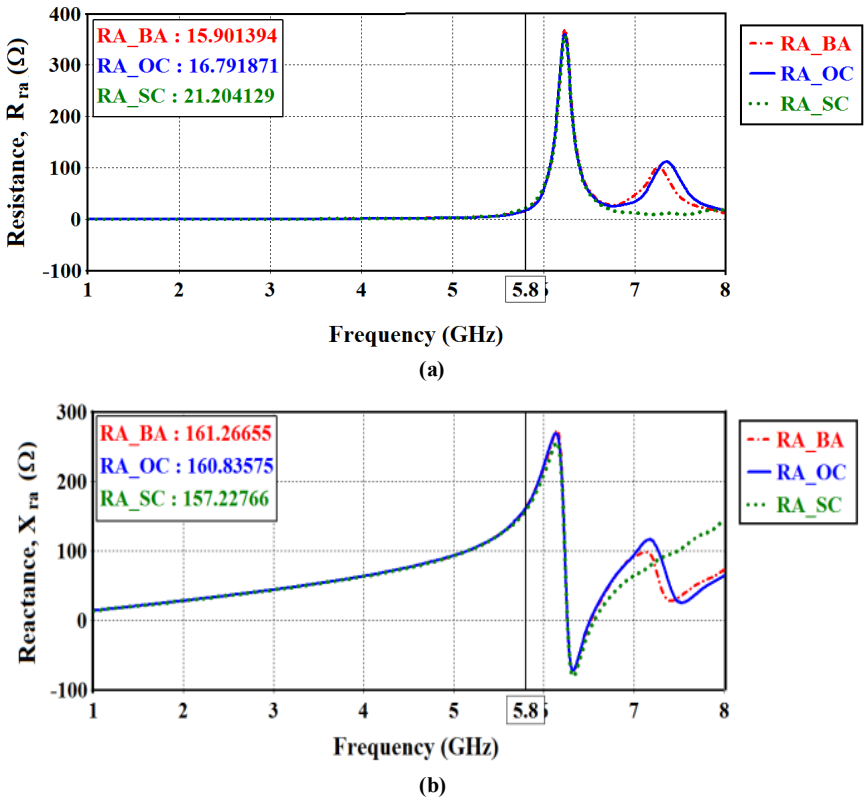

Figure 16. Input resistance (a) and input reactance (b) of the dual-fractal antenna structure when BA is open circuited (BA_OC) or short circuited (BA_SC), and when (RA and BA are ported (RA_BA). Z_{ba}=50 Ω, and Z_{ra}= (10+j160) Ω

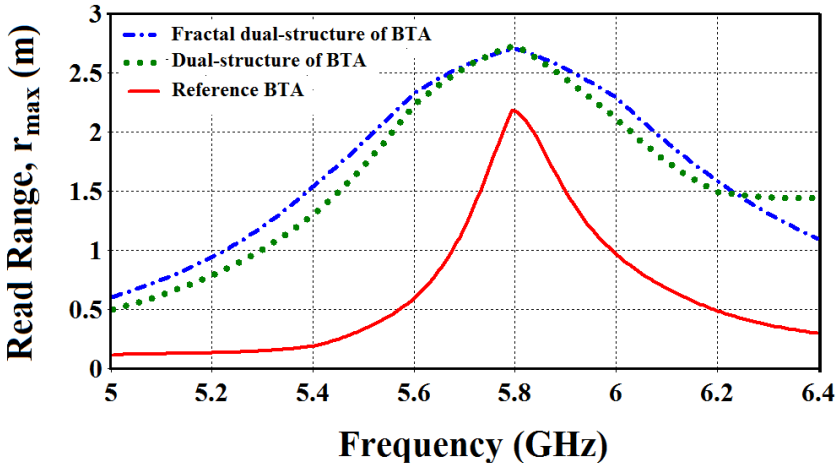

Figure 17. Reading ranges of the miniaturized antennas as a function of frequency

Although there are many different tag performance criteria such as tag orientation sensitivity, chip sensitivity, frequency of operation, etc. the most important one is read range. The tag read range is defined as the maximum distance at which the RFID reader can detect the RFID tag. The reader has a higher sensitivity than the tag and as a result the read range can be considered as the tag response threshold. Furthermore, the read range is also dependant on other factors such as tag orientation and environmental losses[24]. The read range is calculated using the Friis free-space expression eqn. (18)[25]

$$r_{max} = \frac{\lambda}{4\pi}\sqrt{\frac{P_{red}\,G_{red}}{P_{th}}\,G_{tag}\,\tau} \qquad (18)$$

In eqn. (18), λ is the wavelength, P_{red} is the power transmitted by the reader, G_{red} is the gain of the transmitting antenna, G_{tag} is the gain of the tag antenna. The times of P_{red} by G_{tag} is called ERIP (Equivalent Radiated Isotropic Power), P_{th} is the minimum threshold power necessary to turn on the chip, and τ is the power transmission coefficient which is given by

$$\tau = 1 - |\Gamma|^2 = \frac{4R_cR_a}{|Z_C+Z_a|^2}, \quad 0 \le \tau \le 1 \qquad (19)$$

In eqn. (18), Z_C represents the chip impedance $(R_c\text{-}jX_c)$ and Z_a represents the antenna impedance (R_a+jX_a). In addition, when maximum power is transferred the antenna is said to be perfectly matched to the chip impedance at a particular frequency.

The reading ranges for each of the designed antennas, reference BTA and conventional and fractal dual-structure BTAs are calculated over the operating frequency range using eqn. (18). The results are displayed in Figure 17 for value of ERIP = 3.2 W and threshold power Pth = 10 μW. It can be observed that all RFID tags are functional across the entire ISM frequency band of 5.725–5.875 GHz. At 5.8 GHz, the reading ranges are 2.18, 2.7, and 2.7m for reference BTA, conventional and fractal dual-structure BTAs, respectively.

7. Conclusions

Dual-antenna structures (DASs) for 5.8 GHz RFID systems have been proposed and simulated using conventional and fractal bow-tie patch geometries. An optimization-based approach is introduced to miniaturize the proposed DAS which consists of two antennas, one is the receiving antenna at the upper side, and the other one is the backscattering antenna at the other side. Two objective functions are used to satisfy the design requirements of the proposed dual structure, one for conjugate matching the receiving antenna to the IC chip and to make the input impedance of the backscattering antenna pure real, and the other objective function is to minimize structure area. A compact size 3rd-order DAS structure is achieved from the optimization approach (13.93 X 13.23 mm2 or 0.27 X 0.25 λ2 at 5.8 GHz) Because of the low mutual coupling, the backscattering antenna performance is not affected by loading the receiving antenna. Also, the receiving antenna performance nearly does not change by loading the backscattering antenna by the two states of loading, short or open circuit.

REFERENCES

[1] K. Finkenzeller, RFID Handbook, 3rd ed. New York, NY, USA: Wiley, 2010.

[2] A. G. Santiago, J. R. Costa, and C. A. Fernandes, "Broadband UHF RFID passive tag antenna for near-body applications", IEEE Antennas and Wireless Propag. Lett. vol. 12, pp. 136-139, 2013.

[3] P. Hajizadeh, H. R. Hassani, and S. H. Sedighy, "Planar artificial transmission lines loading for miniaturization of RFID printed quasi-Yagi antenna", IEEE Antennas and Wireless Propag. Lett. vol. 12, pp. 464-467, 2013.

[4] K.-H. Lin, S.-L. Chen, and R. Mittra, "A looped-bowtie RFID tag antenna design for metallic objects", IEEE Trans. on Antennas and Propag., vol. 61, no. 2, pp. 499-505, Feb. 2013.

[5] X. Jian, X. Zeng, and L. Zhang, "An innovative semicircular spiral antenna for on-metal passive RFID applications", IEEE Trans. on Antennas and Propag., vol. 61, no. 3, pp. 1026-1031,

March 2013.

[6] A. Lazaro, A. Ramos, R. Villarino, and D. Girbau, "Time-domain UWB RFID tag based on reflection amplifier", IEEE Trans. on Antennas and Propag., vol. 12, pp. 520-523, 2013.

[7] E. A. Soliman, M. O. Sallam, W. D. Raedt, and G. A. E. Vandenbosch, "Miniaturized RFID tag antenna operating at 915 MHz", IEEE Antennas and Wireless Propag. Lett. vol. 11, pp. 1068-1071, 2012.

[8] A. E. Abdulhadi, and R. Abhari, "Design and experimental evaluation of miniaturized monopole UHF RFID tag antennas", IEEE Antennas and Wireless Propag. Lett. vol. 11, pp. 248-251, 2012.

[9] J.-K. Byun, N.-S. Choi and D.-H. Kim, "Optimal design of a RFID tag antenna based on plane-wave incidence", IEEE Trans. on Magnetics, vol. 48, no. 2, pp. 795-798, Feb. 2012.

[10] D. Kim, and J. Yeo, "Dual-band long-range passive RFID tag antenna using an AMC ground plane", IEEE Trans. on Antennas and Propag., vol. 60, no. 6, pp. 2620-2626, June 2012.

[11] Y.-F. Lin, S.-A. Yeh, H.-M. Chen and S.-W. Chang, "Design of an omnidirectional polarized RFID tag antenna for safety glass applications", IEEE Trans. on Antennas and Propag., vol. 60, no. 10, pp. 4530-4537, Oct. 2012.

[12] L. Catarinucci, R. Colella, and L. Tarricone, "Enhanced UHF RFID sensor-tag", IEEE Microwave and Wireless Comp. Lett., vol. 23, no. 1, pp. 49-51, Jan. 2013.

[13] J. Essel, D. Brenk, J. Heidrich, R. Weigel, and D. Kissinger, "Large-signal measurements and nonlinear characterization of an analog frontend for passive UHF CMOS RFID transponders", IEEE Trans. on Microwave Theory and Techniques, vol. 61, no. 2, pp. 948-959, Feb. 2013.

[14] M. Polivka, A. Holub, M. Vyhnalik, and M. Svanda, "Impedance properties and radiation efficiency of electrically small double and triple split-ring antennas for UHF RFID applications", IEEE Antennas and Wireless Propag. Lett. vol. 12, pp. 221-224, 2013.

[15] Y.-S. Chen, S.-Y. Chen and H.-J. Li, "A novel dual-antenna structure for UHF RFID tags", IEEE Trans. on Antennas and Propag., vol. 59, no. 11, pp. 3950-3960, Nov. 2011.

[16] H.-D. Chen, C.-Y.-D. Sim and S.-H. Kuo, "Compact broadband dual coupling-feed circularly polarized RFID microstrip tag antenna", IEEE Trans. on Antennas and Propag., vol. 60, no. 12, pp. 5571-5577, Dec.. 2012.

[17] T. Bauernfeind, K. Preis, G. Koczka, S. Maier, and O. Biro, "Influence of the non-linear UHF-RFID IC impedance on the backscatter abilities of a T-match tag antenna design", IEEE Trans. on Magnetics, vol. 48, no. 2, pp. 755-758, Feb. 2012.

[18] A. Azari, "A new super wideband fractal microstrip antenna", IEEE Trans. on Antennas and Propag. vol. 59, no. 5, pp. 1724-1727, Ma, 2011.

[19] D. Li, and J.-f. Mao, "A Koch-like sided fractal bow-tie dipole antenna", IEEE Trans. on Antennas and Propag. vol. 60, no. 5, pp. 2242-2252, May, 2012.

[20] P.V. Nikitin, K.V. S. Rao and R.D. Martinez, "Differential RCS of RFID tag", Electronics Lett., vol. 43, no. 8, April, 2007

[21] A. C. Durgun, C. A. Balanis, C. R. Birtcher, and D. R. Allee, "Design, simulation, fabrication and testing of flexible bow-tie antennas", IEEE Trans. on Antennas and Propag., vol. 59, no. 12, pp. 4425-4435, Dec., 2011.

[22] J. Nanbo, and R-S. Yahya, "Advances in particle swarm optimization for antenna designs: real-number, binary, single-objective and multi-objective implementation", IEEE Trans. on Antennas and Propag. vol. 55, no. 3, Mar. 2007.

[23] A. Mehdipour, I. D. Rosca, A. - R. Sebak, C. W. Trueman, and S. V. Hoa, "Full - composite fractal antenna using Carbon nanotubes for multiband wireless applications", IEEE Antennas and Wireless Propag. Lett. vol. 9, pp. 891 - 894, Sep. 2010.

[24] K.V.S. Rao, P.V. Nikitin, and S. Lam, "Antenna design for UHF RFID tags: a review and a practical application", IEEE Trans. on Antennas and Propag., vol. 53, pp. 3870-3876, Dec. 2005.

[25] P. V. Nikitin, K. V. S. Rao, S. F. Lam, V. Pillai, R. Martinez, and H. Heinrich, "Power reflection coefficient analysis for complex impedances in RFID tag design", IEEE Transactions on Microwave Theory and Techniques, vol. 53, no. 9, pp. 2721–2725, Sep. 2005.